Earth and Planetary Science Letters 439 (2016) 158–171

Contents lists available at ScienceDirect

Earth and Planetary Science Letters

www.elsevier.com/locate/epsl

Improving the *Ginkgo* CO_2 barometer: Implications for the early Cenozoic atmosphere

Richard S. Barclay *, Scott L. Wing

Department of Paleobiology, National Museum of Natural History, Smithsonian Institution, 10th & Constitution, Washington, DC, 20560-0121, USA

ARTICLE INFO

Article history:
Received 15 May 2015
Received in revised form 8 January 2016
Accepted 13 January 2016
Available online 3 February 2016
Editor: H. Stoll

Keywords:
stomatal index
Ginkgo biloba
improved response curve
total diffusivity
carbon dioxide
greenhouse climate

ABSTRACT

Stomatal properties of fossil *Ginkgo* have been used widely to infer the atmospheric concentration of CO_2 in the geological past (paleo-pCO_2). Many of these estimates of paleo-pCO_2 have relied on the inverse correlation between pCO_2 and stomatal index (*SI* – the proportion of epidermal cells that are stomata) observed in recent *Ginkgo biloba*, and therefore depend on the accuracy of this relationship. The *SI*-pCO_2 relationship in *G. biloba* has not been well documented, however.

Here we present new measurements of *SI* for leaves of *G. biloba* that grew under pCO_2 from 290 to 430 ppm. We prepared and imaged all specimens using a consistent procedure and photo-documented each count. As in prior studies, we found a significant inverse relationship between *SI* and pCO_2, however, the relationship is more linear, has a shallower slope, and a lower correlation coefficient than previously reported. We examined leaves of *G. biloba* grown under pCO_2 of 1500 ppm, but found they had highly variable *SI* and a large proportion of malformed stomata. We also measured stomatal dimensions, stomatal density, and the carbon isotope composition of *G. biloba* leaves in order to test a mechanistic model for inferring pCO_2. This model overestimated observed pCO_2, performing less well than the *SI* method between 290 and 430 ppm.

We used our revised SI-pCO_2 response curve, and new observations of selected fossils, to estimate late Cretaceous and Cenozoic pCO_2 from fossil *Ginkgo adiantoides*. All but one of the new estimates is below 800 ppm, and together they show little long-term change in pCO_2 or relation to global temperature. The low Paleogene pCO_2 levels indicated by the *Ginkgo SI* proxy are not consistent with the high pCO_2 inferred by some climate and carbon cycle models. We cannot currently resolve the discrepancy, but greater agreement between proxy data and models may come from a better understanding of the stomatal response of *G. biloba* to elevated pCO_2, better counts and measurements of fossil *Ginkgo*, or models that can simulate greenhouse climates at lower pCO_2.

1. Introduction

Reconstructing the relationship between atmospheric composition and global climate remains a fundamental problem in earth science and a matter of pressing societal concern as well. For most of the last 200 million years, Earth's climate has been much warmer than at present. This is widely thought to result from higher than present concentrations of CO_2 in the atmosphere (pCO_2), but proxies for pCO_2 prior to ice-core records (ca. 800 ka) produce a large range of estimates, particularly before the Miocene (Beerling and Royer, 2011).

Stomatal frequency in fossil plants has been used widely to infer ancient pCO_2, usually by reference to a correlation established in recent plants (Woodward, 1987). In this approach, stomatal index (*SI* – the proportion of epidermal cells that are stomatal complexes) or stomatal density (SD_{ab} – the number of stomata per unit area of abaxial leaf surface) is measured on leaves that grew under a range of pCO_2, and the correlation curve of *SI* or SD_{ab} with pCO_2 is then used to estimate ancient pCO_2 from the stomatal frequency of fossil leaves (Van der Burgh et al., 1993). Underlying this method is the tradeoff between water loss and CO_2 uptake that applies to all photosynthetic land plants – under higher pCO_2 many plants reduce stomatal frequency, thus reducing water loss but still acquiring enough CO_2 to photosynthesize at the same rate (Woodward, 1987). This response has been shown in individual long-lived plants (Wagner et al., 1996), within species (Van der Burgh et al., 1993), and in whole forests (Beerling and Kelly, 1997) during the anthropogenic rise in pCO_2. SD_{ab} varies more than *SI* on individual plants (Chen et al., 2001) because it is area-dependent and therefore susceptible to environmental factors that influence epidermal cell expansion (Kürschner et al., 1996).

* Corresponding author.
E-mail address: barclay.rich@gmail.com (R.S. Barclay).

http://dx.doi.org/10.1016/j.epsl.2016.01.012
0012-821X/

The *SI* method has been tested by comparing pCO_2 estimates made from *SI* of Quaternary fossils with measurements of pCO_2 in coeval ice-core bubbles (van de Water et al., 1994; Wagner et al., 1999; Rundgren and Bennike, 2002). Agreement is generally good (Steinthorsdottir et al., 2013), though *SI* estimates fluctuate more than ice-core measurements, possibly because of different amounts of time-averaging (van Hoof et al., 2005).

Many estimates of pCO_2 for the Late Cretaceous and Cenozoic rely on the relationship between *SI* and pCO_2 in extant *Ginkgo biloba*, though images and raw data documenting the correlation have not been published (Retallack, 2001; Royer et al., 2001) and original specimens are not available (Beerling, pers. comm., 2014). *G. biloba* is especially useful for reconstructing Late Cretaceous and Cenozoic pCO_2 because the common fossil species *Ginkgo adiantoides* is morphologically and ecologically very similar to extant *G. biloba* (Tralau, 1968; Royer, 2003; Royer et al., 2003), justifying the assumption that the two species have the same response to changing pCO_2. *G. biloba* has also been used in developing mechanistic biophysical models of leaf diffusivity that are used to estimate the pCO_2 of the atmosphere from anatomical features of stomata and the carbon isotope composition of the leaf (Grein et al., 2011; Franks et al., 2014; Roth-Nebelsick et al., 2014).

The work we present here is directed at improving the methods by which *SI* is studied and documented in *Ginkgo*, and at testing the accuracy and precision of pCO_2 estimates made using response curves and a mechanistic model. We also recalculate Late Cretaceous and Cenozoic pCO_2 estimates using our revised *SI* response curve for *Ginkgo* and a small number of new observations of fossils. Although other fossil ginkgoaleans have been used to estimate pCO_2 during the earlier Mesozoic, we did not treat these in our study because these older species are anatomically and morphologically distinct from *G. biloba*, which makes the assumption that they share the same *SI* response curve more tenuous.

2. Materials and methods

2.1. Sample collection

Leaf specimens from historical collections of *G. biloba* were sampled from 29 herbarium sheets (Table 1) at the National Arboretum Herbarium and the Herbarium of the National Museum of Natural History. To reduce sampling impact on herbarium sheets we sliced a 1/2 cm square from the distal leaf center (no margin), taking replicates where material allowed.

Leaves were also collected from living *G. biloba* trees (Table 1), one outdoors at Blandy Experimental Farm (Virginia) and one on the grounds of the Library of Congress (facing 2nd Street SE) in Washington, D.C. We collected five leaves each from short shoots on branches of mature male trees at ~2 m height on the unshaded south side. Leaves were placed directly into envelopes and air dried. To study variability in stomatal frequency within leaves we sampled five leaves from a single short shoot of the tree on the Library of Congress grounds in four equivalent locations: distal on the right lobe, midline below the sinus, central on the right side, and basal on the leaf (20 samples total). Finally, we sampled six plants from the CO_2 experiment of Haworth et al. (2013), three each from the control and elevated treatments (2 leaves per plant; 12 total; Table 1).

2.2. Cuticle preparation, imaging, and measurement

All *G. biloba* cuticle was prepared using the same method. Dried leaves were macerated using a three-step chemical process to separate upper from lower cuticle. Samples were placed in glass vials filled with DI water, and soaked for 24 h. DI water was replaced with HCl (5% v/v) for 48 h. Samples were neutralized and placed into 20 mL of aqueous hexavalent chromium [1 g $Cr(VI)O_3$ per 4 mL water].

Cuticle pieces were mounted on 12 mm SEM stubs with the internal side facing upwards, then air dried on ultra-smooth carbon adhesive tabs. Uncoated specimens were imaged at 32 Pa in a Carl Zeiss EVO-MA15 environmental SEM at the National Museum of Natural History (NMNH, Smithsonian) in Washington D.C. The voltage target was 15 kV, with an ion probe at 900 pA, and a working distance of 8–10 mm. We used only the top two backscatter detectors to create shadows and highlight micro-topography. Seven random interveinal areas on the lower cuticle of each specimen were imaged at ×200, where the preparations were clean and epidermal cell outlines distinct. Images were captured as .TIFs (3 min cycle, typically 3072 × 2454 pixels).

All epidermal cell counts and measurements were conducted on SEM images using ImageJ (ver. 1.47v), including stomatal density (SD_{ab}: number of stomata per mm^2), *SI*, and stomatal dimensions (pore length = Gcl_{ab}; stomatal apparatus width = 2 × *Gcw*). All counts were within 300 × 300 micron areas, avoiding veins. For SD_{ab} and *SI* counts, the ImageJ cell-counter plugin was used to document and annotate counts within .xml files, which can be reloaded and modified in ImageJ. The final counted image was saved as a .JPEG. Stomata and cells that intersected any part of the 300 × 300 µm box were counted as 'in', which is the procedure required by the total diffusivity methodology (Franks et al., 2014). *G. biloba* has anomocytic stomatal complexes (no differentiation of subsidiary cells), so all epidermal cells (except guard cells) were used to calculate *SI*, which was the procedure used to create previous calibration curves (Royer, pers. comm., 2014).

Gcl_{ab} and *Gcw* were required for estimating pCO_2 using the total diffusivity model. Images were calibrated within ImageJ using the SEM scale bar. Measurements were made on all stomata for which pore length and guard cell width were completely visible. Images of measurements (with count-labels) were saved as .JPEGs. The width of both guard cells (outer edge to outer edge) was measured perpendicular to the axis of pore length.

2.3. Determination of pCO_2

Observed pCO_2 was determined by different methods for different plants. For herbarium specimens collected before 1959, pCO_2 was assigned the global average estimated from ice-core bubbles (Neftel et al., 1985; Friedli et al., 1986). For herbarium specimens collected after 1959 and for leaves collected from living trees at Blandy, we used annual global average pCO_2 measured at Mauna Loa (Keeling et al., 2005). For leaves sampled from trees growing outside in Washington D.C., we measured pCO_2 at 5-min intervals during 2013 and 2014 at NMNH. The 2-yr mean was 430 ppm (Fig. S1). We used the pCO_2 values reported in Haworth et al. (2013) for growth chamber material. The paleo-elevation of the Eocene Falkland Site was estimated at 1300 m (Smith et al., 2010), but all other data are from close to sea level, so the pCO_2 from this site was corrected to sea-level using the methodology of Kürschner et al. (2008).

2.4. Isotopic measurements

Carbon isotope values were determined from 0.2 to 0.3 mg of cleaned but otherwise untreated leaves. Isotope ratios were measured using a Costech ECS 4010 combustion EA connected via continuous flow through a Thermo Conflo IV to a Thermo Delta-V-Advantage IRMS, at the Museum Conservation Institute (Smithsonian). All calculations of raw isotope values were performed with Isodat 2.8 software, corrected using calibrated acetanilide (Costech) and urea (UIN31) standards, both calibrated to USGS40 and USGS41 (L-glutamic acids). Runs included 10 standards per

Table 1
Locality information for samples of *Ginkgo biloba* used in this study. Distance from Smithsonian in Washington, D.C. measured using Google Earth (ver. 7.1.2.2041).

Date collected	Herbarium	Sample number	Leaf	Site	City	State	km to D.C.	CO_2 (ppm)
5/24/1877	US	57 339	A	Dept. Agriculture Grounds	Washington	D.C.	0	290
1888	US	57 342	A/B	US Botanic Garden	Washington	D.C.	1	293
8/27/1896	US	57 363	A/B	Dept. Agriculture Grounds	Washington	D.C.	0	295
10/1/1904	NA	15 089	A	–	Vineland	NJ	190	296
8/1920	NA	15 049	A/B	Dept. Agriculture Grounds	Washington	D.C.	0	301
5/29/1928	NA	3804	A	Maymont Park	Richmond	VA	154	306
10/10/1931	NA	15 088	A	Catholic Univ. of Amer.	Washington	D.C.	6	306
10/26/1936	US	227 512	A/B	Dept. Agriculture Grounds	Washington	D.C.	0	307
11/29/1942	NA	3805	A	Private Garden	Berkeley	CA	3900	308
11/12/1959	NA	15 101	A/B	Arlington Cemetery	Arlington	VA	4	316
7/22/1964	NA	15 085	A	Shenandoah Nat'l Pk.	–	VA	143	320
6/25/1968	NA	15 024	A/B	Mt. Cuba Bot. Pk.	Greenville	DE	153	323
8/22/1968	NA	15 025	A/B	Mt. Cuba Bot. Pk.	Greenville	DE	153	323
10/9/1968	NA	15 030	A	Arnold Arboretum	Cambridge	MA	630	323
10/15/1968	NA	3806	A	Arnold Arboretum	Cambridge	MA	630	323
10/23/1969	NA	15 064	A/B	Maymont Park	Richmond	VA	153	325
7/19/1973	NA	15 073	A/B	Maymont Park	Richmond	VA	153	330
7/17/1974	NA	15 096	A/B	Goochland County	Manakin	VA	150	330
8/26/1977	NA	3809	A	Library of Congress	Washington	D.C.	2	334
10/9/1977	NA	3807	A/B	Blandy Experimental Farm	Boyce	VA	91	334
7/1/1980	NA	15 069	A	White House	Washington	D.C.	1	339
6/30/1987	NA	3808	A	Morton Arboretum	Lisle	IL	990	349
11/27/1993	NA	15 055	A	13 W. 2nd St.	Frederick	MD	67	357
9/27/2012	Barclay coll.	RSB1272	A–E	Blandy Experimental Farm	Boyce	VA	91	394
9/27/2012	Barclay coll.	RSB1273	A	Blandy Experimental Farm	Boyce	VA	91	394
9/27/2012	Barclay coll.	RSB1274	A–E	Blandy Experimental Farm	Boyce	VA	91	394
10/8/2013	Barclay coll.	RSB1343	A–E	Library of Congress, 2nd St.	Washington	D.C.	2	429
2013	UCD Chamber	RSB1432_Gb1A	R17	University College Dublin	Dublin	Ireland	–	380
2013	UCD Chamber	RSB1433_Gb1A	R33	University College Dublin	Dublin	Ireland	–	380
2013	UCD Chamber	RSB1435_Gb2A	R50	University College Dublin	Dublin	Ireland	–	380
2013	UCD Chamber	RSB1434_Gb2A	R60	University College Dublin	Dublin	Ireland	–	380
2013	UCD Chamber	RSB1436_Gb3A	R10	University College Dublin	Dublin	Ireland	–	380
2013	UCD Chamber	RSB1437_Gb3A	R20	University College Dublin	Dublin	Ireland	–	380
2013	UCD Chamber	RSB1438_Gb1D	R21	University College Dublin	Dublin	Ireland	–	1500
2013	UCD Chamber	RSB1439_Gb1D	R50	University College Dublin	Dublin	Ireland	–	1500
2013	UCD Chamber	RSB1441_Gb2D	R33	University College Dublin	Dublin	Ireland	–	1500
2013	UCD Chamber	RSB1440_Gb2D	R57	University College Dublin	Dublin	Ireland	–	1500
2013	UCD Chamber	RSB1442_Gb3D	17	University College Dublin	Dublin	Ireland	–	1500
2013	UCD Chamber	RSB1443_Gb3D	12	University College Dublin	Dublin	Ireland	–	1500

38 samples, run with the same parameters and procedures as the samples, except that CO_2 peaks were quantitatively diluted by 65% (standards) and 35% (samples). Reproducibility of standards is $\leq 0.2‰$ (1σ).

2.5. Numerical analyses

We estimated pCO_2 from stomatal features using three different methods: the total diffusivity model of Franks et al. (2014); linear and curvilinear regression with *SI* as the predictor; and multiple regression using four predictor variables: mean SD_{ab} (equals D_{ab} used by Franks et al., 2014), leaf carbon isotope discrimination ($\Delta^{13}C_{leaf}$), mean Gcl_{ab}, and mean Gcw_{ab}. All statistical analyses were conducted using the R base package (v.2.15.3; R core team, 2013). Simple and multiple linear regression analyses were conducted using the lm command; the power-curve was fit to data using the nls command; the aov command was used to conduct a repeated measures ANOVA in the test of *SI* variability within individual leaves.

To apply the total diffusivity model of Franks et al. (2014) we used the R script they provided to calculate pCO_2 from our stomatal measurements. There were 13 variables in the total diffusivity model. Following procedure, we measured SD_{ab}, $\Delta^{13}C_{leaf}$, Gcl_{ab}, and Gcw_{ab} for this study. Nine other variables were used in the model. Fortunately, values for the variables in *G. biloba* were provided by Franks et al. (2014). To facilitate comparison with the model variables of Franks et al. (2014), we use their abbreviations, with the standard mean error in parentheses: 1) pCO_2: CO2_O = 390 ppm (0); 2) photosynthetic rate at CO2_0: $A_0 = 5.85$ (0.09); 3) boundary layer conductance to CO_2: $g_b = 2$ (0.1); 4) ratio of guard cell length to pore length (alpha): s1 = 1 (0); 5) ratio of single guard cell width to pore depth: s2 = 1 (0.05); 6) scaling from pore length to maximum area of stomatal pore (beta): s3 = 0.6 (0.025); 7) scaling from maximum conductance to CO_2 (g_{cmax}) to operational conductance to CO_2 (zeta): s4 = 0.21 (0.01); 8) scaling from photosynthetic rate to mesophyll conductance to CO_2: s5 = 0.013 (0.00065). 9) The carbon isotope composition of the atmosphere ($\delta^{13}C_a$) for each specimen is based upon the year collected (Friedli et al., 1986; Keeling et al., 2005; Table 2). Following Franks et al. (2014), we assigned zero error to $\delta^{13}C_a$.

3. Results

3.1. Preparation of Ginkgo cuticle

We tried several techniques for preparing *G. biloba* leaves in order to count stomata and measure epidermal features, including epifluorescence microscopy as described by Royer et al. (2001). We found it difficult to distinguish epidermal cells under epifluorescent light because cell borders were indistinct or obscured by papillae; even stomata were difficult to recognize. Using different light filters did not change this result. Representative images of cuticles prepared using several techniques are shown in Fig. 1.

Chemical maceration followed by SEM (see Section 2) produced by far the clearest cell outlines, so all counts and measurements for this study were made on specimens prepared using this technique (Fig. 2). Unaltered images, and images documenting all counts and

Table 2
Mean values for stomatal index (*SI*), stomatal density (SD_{ab}), pore length (Gcl_{ab}), single guard cell width (Gcw_{ab}), and stable carbon isotope value ($\delta^{13}C_p$) for each *Ginkgo biloba* leaf. The carbon isotope composition of air ($\delta^{13}C_a$) for experimental studies was depleted relative to normal atmosphere because of addition of CO_2 with low isotopic composition. Error is 0.2‰, equivalent to the error on the standards. Abbreviations: nd = no data.

Date collected	Sample No.	Leaf No.*	*SI*/ SD_{ab} No.◆◆	Mean SD_{ab}	SD_{ab} s.e.m.	SD_{ab} σ	Mean *SI*	*SI* s.e.m.	*SI* σ	Mean ED	Franks model n‡	Franks model N◆◆	*Gcl* (μm)	*Gcl* s.e.m.	Single *Gcw* (μm)	*Gcw* s.e.m.	$\delta^{13}C_p$ (vpdb)
5/24/1877	57 339	A	10	170.0	7.95	25.1	10.28	0.26	0.82	1481	7	137	10.60	0.76	12.44	0.44	nd
1888	57 342	A	6	183.3	13.07	32.0	10.38	0.45	1.11	1574	7	37	11.00	1.13	14.17	0.66	nd
1888	57 342	B	5	184.4	12.96	29.0	10.03	0.40	0.81	1658	6	44	11.38	1.01	14.25	0.63	nd
8/27/1896	57 363	A	7	190.5	5.10	13.5	10.63	0.34	0.89	1605	7	115	14.99	1.46	16.82	0.72	nd
8/27/1896	57 363	B	7	193.7	4.76	12.6	9.55	0.17	0.45	1833	7	79	12.31	0.93	16.76	0.66	nd
10/1/1904	15 089	A	7	104.8	4.10	10.8	8.69	0.35	0.93	1103	7	55	13.16	1.19	16.71	0.60	−25.07
8/1920	15 049	A	7	120.6	5.10	13.5	9.13	0.28	0.75	1200	7	97	14.56	1.05	15.76	0.62	−27.78
8/1920	15 049	B	6	125.9	6.83	16.7	9.26	0.48	1.17	1237	6	83	13.71	1.32	14.29	0.59	nd
5/29/1928	3804	A	9	182.7	7.43	22.3	9.81	0.18	0.50	1627	7	115	11.59	0.79	13.90	0.44	−25.65
10/10/1931	15 088	A	7	179.4	2.90	7.7	9.38	0.13	0.33	1735	7	95	11.41	0.99	14.69	0.62	−25.26
10/26/1936	227 512	A	7	193.7	8.69	23.0	10.29	0.47	1.23	1690	7	131	13.01	0.92	15.48	0.69	nd
10/26/1936	227 512	B	7	168.3	8.20	21.7	9.90	0.30	0.79	1529	7	98	13.30	1.13	16.21	0.74	nd
11/29/1942	3805	A	7	149.2	11.59	30.7	9.66	0.69	1.82	1394	7	71	11.30	0.89	13.90	0.64	−27.38
11/12/1959	15 101	A/B	7	120.6	4.49	11.9	9.12	0.23	0.61	1200	7	119	17.90	1.26	14.83	0.75	−26.83
7/22/1964	15 085	A	7	130.2	7.16	18.9	9.38	0.38	1.00	1256	7	108	15.79	1.28	15.64	0.77	−27.95
6/25/1968	15 024	A/B	7	146.0	7.04	18.6	9.42	0.37	0.99	1403	7	60	14.47	1.26	15.26	0.69	−27.24
8/22/1968	15 025	A/B	7	177.8	4.85	12.8	9.78	0.18	0.47	1638	7	145	13.99	0.96	15.57	0.75	−28.62
10/9/1968	15 030	A	7	158.7	5.26	13.9	9.81	0.28	0.74	1460	7	98	14.72	1.76	16.03	0.68	−27.01
10/15/1968	3806	A	7	117.5	9.95	26.3	8.91	0.43	1.14	1190	7	104	13.84	1.07	15.12	0.66	−27.59
10/23/1969	15 064	A/B	7	131.7	7.04	18.6	9.28	0.42	1.11	1286	7	114	16.88	1.25	15.61	0.64	−25.42
7/19/1973	15 073	A/B	6	161.1	6.25	15.3	9.85	0.24	0.59	1472	7	94	13.61	1.78	15.12	0.61	−26.58
7/17/1974	15 096	A/B	7	115.9	6.35	16.8	8.98	0.47	1.25	1175	7	81	14.45	1.52	15.29	0.90	−26.97
8/26/1977	3809	A	7	138.1	5.34	14.1	9.33	0.24	0.63	1341	7	129	15.90	1.12	17.27	0.54	−27.06
10/9/1977	3807	A	6	146.3	5.30	13.0	9.67	0.38	0.93	1369	6	48	11.93	1.46	15.30	0.80	−26.35
10/9/1977	3807	B	7	115.9	11.07	29.3	9.48	0.49	1.30	1092	7	72	13.56	1.47	15.32	0.66	nd
7/1/1980	15 069	A	7	195.2	10.80	28.6	9.32	0.31	0.82	1895	7	51	9.88	0.88	12.23	0.46	−26.68
6/30/1987	3808	A	7	111.1	4.85	12.8	8.69	0.18	0.44	1130	7	96	15.21	1.13	16.18	0.73	−27.53
11/27/1993	15 055	A	6	124.1	6.68	16.4	9.33	0.24	0.60	1206	7	121	16.88	2.05	15.68	0.89	nd
9/27/2012	RSB1273A	A	7	114.3	6.28	16.6	8.45	0.35	0.92	1235	nd	nd	nd	nd	nd	nd	−29.27
9/27/2012	RSB1274A	A	7	104.8	4.10	10.8	8.53	0.33	0.88	1125	7	117	17.21	1.62	14.32	0.70	−29.34
9/27/2012	RSB1274B	B	7	100.0	6.42	17.0	8.23	0.39	1.03	1113	7	111	16.64	1.65	14.26	0.73	−29.01
9/27/2012	RSB1274C	C	7	100.0	5.94	15.7	8.33	0.39	1.03	1100	7	111	17.28	1.62	14.03	0.81	−28.58
9/27/2012	RSB1274D	D	7	111.1	9.07	24.0	8.66	0.48	1.27	1162	7	117	17.64	1.56	15.01	0.74	−27.93
9/27/2012	RSB1274E	E	7	95.2	10.25	27.1	8.23	0.64	1.70	1049	7	89	16.38	1.35	14.30	0.81	nd
10/8/2013	RSB1343A	A	7	93.7	8.69	23.0	8.64	0.61	1.61	979	7	103	15.86	1.53	14.58	0.75	−27.23
10/8/2013	RSB1343B	B	6	87.0	6.03	14.8	8.01	0.42	1.02	996	6	56	15.69	1.48	14.87	0.97	−26.71
10/8/2013	RSB1343C	C	7	87.3	7.83	20.7	8.63	0.54	1.42	916	7	84	16.01	1.24	14.82	0.98	−27.35
10/8/2013	RSB1343D	D	7	115.9	4.10	10.8	9.14	0.22	0.57	1154	7	116	14.31	1.50	14.63	0.85	−27.55
10/8/2013	RSB1343E	E	7	95.2	7.61	20.1	8.47	0.46	1.21	1027	7	103	17.03	1.74	14.61	0.76	−26.63
2013	RSB1432_Gb1A	R17	7	79.4	6.15	16.3	8.87	0.49	1.29	810	nd	nd	nd	nd	nd	nd	−32.76
2013	RSB1433_Gb1A	R33	6	164.8	6.68	16.4	13.06	0.30	0.74	1098	nd	nd	nd	nd	nd	nd	−34.29
2013	RSB1435_Gb2A	R50	7	111.1	6.42	17.0	8.99	0.42	1.12	1122	nd	nd	nd	nd	nd	nd	−31.17
2013	RSB1434_Gb2A	R60	6	57.4	3.41	8.4	7.90	0.27	0.66	667	nd	nd	nd	nd	nd	nd	−33.84
2013	RSB1436_Gb3A	R10	6	77.8	2.87	7.03	8.25	0.39	0.95	869	nd	nd	nd	nd	nd	nd	−33.38
2013	RSB1437_Gb3A	R20	6	90.7	7.81	19.1	9.02	0.59	1.46	909	nd	nd	nd	nd	nd	nd	−32.80
2013	RSB1438_Gb1D	R21	6	85.2	6.83	16.7	9.24	0.61	1.50	833	nd	nd	nd	nd	nd	nd	−52.69
2013	RSB1439_Gb1D	R50	7	158.7	11.04	29.2	12.30	0.72	1.90	1127	nd	nd	nd	nd	nd	nd	−51.77
2013	RSB1441_Gb2D	R33	4	119.4	6.99	14.0	9.96	0.22	0.43	1078	nd	nd	nd	nd	nd	nd	−52.28
2013	RSB1440_Gb2D	R57	7	157.1	10.69	28.3	13.48	0.66	1.74	1003	nd	nd	nd	nd	nd	nd	−49.17
2013	RSB1442_Gb3D	17	7	88.9	6.42	17.0	9.61	0.54	1.42	832	nd	nd	nd	nd	nd	nd	−53.68
2013	RSB1443_Gb3D	12	8	73.6	6.28	17.8	8.22	0.49	1.38	813	nd	nd	nd	nd	nd	nd	−51.52

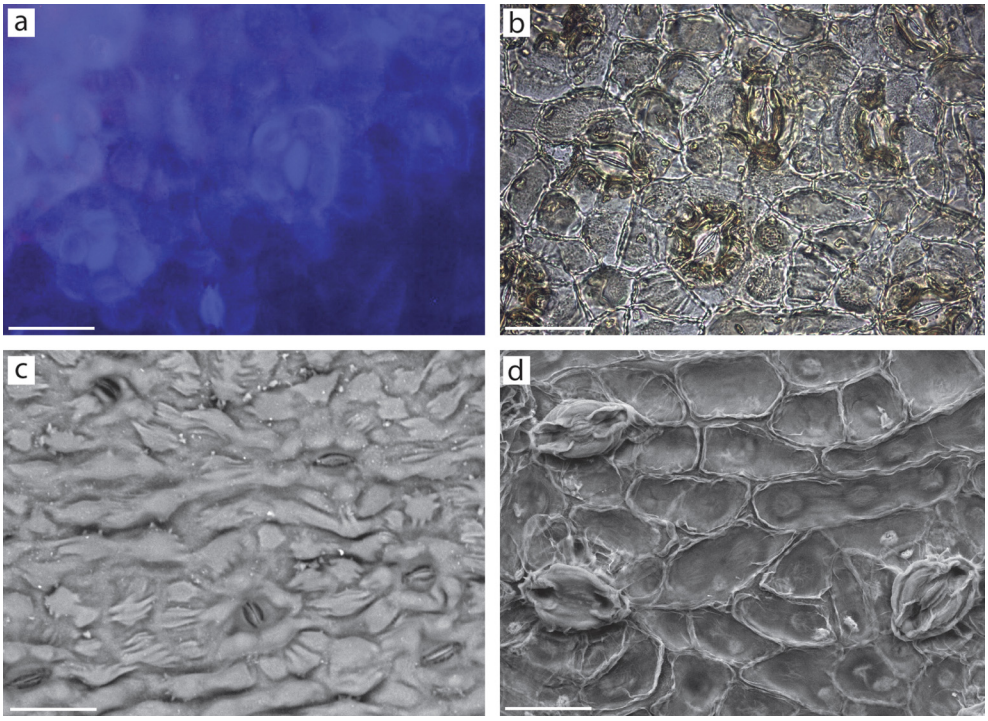

Fig. 1. Images of lower cuticle of *Ginkgo biloba* leaves illustrating the effect of preparation technique and imaging method on cell visibility. (a) Epifluorescence microscope image of lower surface of dried leaf collected in 2012. (b) Transmitted light microscope image of cleared lower cuticle, stained with Bismuth Brown; composite of image stack taken at multiple focus planes through the cuticle. (c) SEM image of outside surface of lower cuticle prepared with $Cr(VI)O_3$. This mimics the best result possible using the acetate peel method. (d) SEM image of internal surface of lower cuticle prepared with $Cr(VI)O_3$. Scale bars: 50 μm.

measurements made for this study are available at the Cuticle Database (http://cuticledb.eesi.psu.edu/; Barclay et al., 2007, 2012).

3.2. Variability in stomatal counts

Individual stomatal counts and measurements made from every leaf image are provided in Tables S1–S3. Six of the herbarium sheets studied by Royer et al. (2001) were resampled from a different leaf and counted for this study (gray symbols in Fig. 3; Table 3). Royer found a higher *SI* than we did for all six specimens (mean difference 1.4, $\sigma = 1.1$), and the discrepancy was larger at higher *SI* values ($r^2 = 0.87$; $p < 0.001$).

To test if leaf region has a significant effect on *SI* in *G. biloba* leaves we conducted a one-way repeated measures ANOVA with the four defined leaf regions as the independent variable and *SI* counts of 140 fields of view (seven fields in each of four regions on each of five leaves) as the dependent variable. We found no significant effect of leaf region [$F = 0.6$ (1,4 d.f.); $p = 0.495$], suggesting that *SI* is homogeneous across leaves of *G. biloba*.

3.3. Stomatal index response curve

The *SI* counts from our preparations of *G. biloba* leaves are strongly and inversely correlated with pCO_2 (Fig. 3). Linear regression of *SI* on pCO_2 is highly significant [$r^2 = 0.58$; $F = 51$ (1,37 d.f.), $p = 1.84 \times 10^{-8}$; $SI = -0.011(pCO_2) + 12.95$], though this slope is much shallower than that observed in previous studies (Fig. 3). Our *SI* data are slightly better fit by a power-curve ($r^2 = 0.60$; $SI = 113.66(pCO_2)^{-0.431}$) than by a straight line (Fig. 3). Most of the trees used in this study grew within 160 km of Washington, D.C., however there are collections from California, Chicago, and Boston (3900 km, 990 km, 630 km away, respectively), which have different climates. If these samples are removed, the fit improves for both the linear regression ($r^2 = 0.67$, $n = 34$) and the power-curve ($r^2 = 0.70$, $n = 34$). The inverse correlation between SD_{ab} and pCO_2 in the full dataset ($n = 39$) is also highly significant ($p = 1.28 \times 10^{-7}$; Fig. S2), but has a lower correlation coefficient than for *SI* (power: $r^2 = 0.57$), and even lower for a linear regression (linear: $r^2 = 0.53$).

3.4. Prediction of pCO_2

We examined the ability of three methods to predict pCO_2 from stomatal features: the two univariate statistical models described above that use *SI* as the predictor, a multiple regression model with four predictor variables, and the total diffusivity model of Franks et al. (2014). For the three statistical models we inverted the regressions (whole dataset; $n = 39$) and considered pCO_2 as the dependent variable. The equation for the linear regression is $pCO_2 = -53.66(SI) + 838.86$ ($r^2 = 0.58$). The power-curve fits the data slightly better, giving the equation $pCO_2 = 9920.9(SI)^{-1.484}$ ($r^2 = 0.60$). The multiple regression approach (Table 2) gives the equation $pCO_2 = 894.3 + [-8.01 \times 10^{-7}(SD_{ab})] + [5.86 \times 10^{6}(Gcl_{ab})] + [-2.14 \times 10^{7}(Gcw_{ab})] + [-10.46(\Delta^{13}C_{leaf})]$; adjusted $r^2 = 0.60$; $F = 10.76$ (4,22 d.f.); $p = 5.474 \times 10^{-5}$. The coefficients for Gcl_{ab} and $\Delta^{13}C_{leaf}$ are not significant at the 0.05 level, but the intercept and coefficients for SD_{ab} and Gcw_{ab} are significant at the 0.01 level or better.

The average absolute value of the residuals is 22.2 ppm for the linear regression and 21.2 ppm for the power-curve regression (Fig. 4). The average residual error for the multiple regression is 21.4 ppm. The residuals for the simple and multiple linear regressions trend slightly positive with increasing pCO_2; those for the power-curve do not have a trend (Fig. 4).

In comparison to the statistical models, the total diffusivity model (Franks et al., 2014) has a larger error and is consistently biased toward over-estimating pCO_2. The average predicted–observed value is 108.8 ± 79.5 ppm. The model also has a strong tendency to over-predict pCO_2 more at lower observed levels of

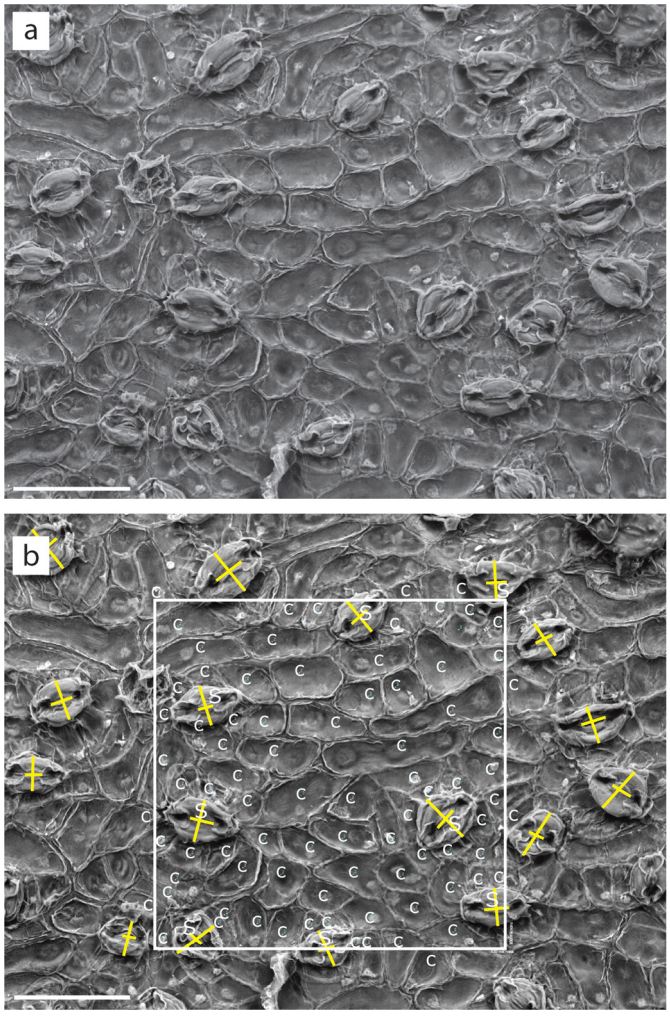

Fig. 2. SEM images of the internal surface of the lower cuticle of *Ginkgo biloba* (RSB1343), collected from a living tree. (a) Unaltered image. (b) Image with stomatal counts and measurements. 300 µm square boxes used for *SI* counts (S = stomata; C = cell). Scale bars 100 µm.

pCO_2. The model produced a single under-estimate, with a calculated pCO_2 of 392.5 ppm for an observed level of 430 ppm.

3.5. Observations on G. biloba grown in chambers

As part of this study we counted *SI* on 12 leaves grown for an experiment by Haworth et al. (2013; Table 2, Fig. 5). We also show the mean values reported by Haworth et al. (2013) for the same plants, and other *SI* values from previous studies of *G. biloba* grown in chambers (Fig. 5; Beerling et al., 1998; Royer et al., 2001). Our data show high variability in *SI* for *G. biloba* grown under both 380 and 1500 ppm pCO_2, with counts spanning nearly the entire range of *SI* values observed in plants grown outdoors (Fig. 3). The mean *SI* value for the six leaves grown at 380 ppm is 9.29 ± 1.9, substantially smaller than the mean of 12.4 ± 2.7 reported by Haworth et al. (2013). The mean for the six leaves at 1500 ppm is 10.47 ± 2.0, compared with 10.3 ± 1.9 reported by Haworth et al. (2013). Relying on both new and previously published observations there is a decline in *SI* from ~9 to ~7 as pCO_2 increases from 380 to 800 ppm, with a single conspicuous outlier among Haworth et al.'s leaves grown at 380 ppm. Our counts of Haworth et al.'s leaves grown at 1500 ppm pCO_2 show that mean *SI* increases at very high pCO_2, but these leaves have highly variable *SI* counts (Fig. 5), and also have highly variable and abnormal stomatal anatomy (see below).

In the course of making counts for *SI*, we observed anatomical differences in stomatal features between field-grown trees and chamber-grown plants. A normally developed stomatal apparatus of *G. biloba* has a pair of guard cells symmetrically arranged around a stomatal pore clearly visible as a slit-like opening (Fig. 6a, Fig. 6b). When viewed from the leaf's interior, guard cells that developed normally are three-dimensional, elongated ellipses, rising above the epidermal pavement. Fully-developed stomatal pores have four ridges (two per guard cell) extending outward from the end of the stomatal pore in a half-moon-arc (Fig. 6a.1, Fig. 6a.2). Less well-developed stomatal complexes may have guard cells that are flattened (Fig. 6e.1, Fig. 6e.2, Fig. 6f.1), asymmetrical, or are small and less distinct in shape (Fig. 6c.2, Fig. 6d.2). More significant abnormalities that would affect the functionality of the stomatal complex include stomatal pores that possibly couldn't function (Fig. 6e.2, Fig. 6f.2), or are holes lacking guard cells (Fig. 6e.3, Fig. 6f.3). The frequency of abnormal stomatal complexes is higher in experimentally grown plants than in field-grown trees (Fig. S3). Leaves from field-grown trees at Blandy (395 ppm) have 15% abnormal stomatal complexes. Chamber-grown plants have either 35% (380 ppm) or 45% (1500 ppm) abnormal stomatal complexes. The difference between the specimens from Blandy and those grown at 1500 ppm is significant ($p = 0.03$, two-tailed t-test).

4. Discussion

4.1. Recommendations for observing Ginkgo cuticle and measuring SI

We suggest three basic improvements for studying *SI* and other stomatal features in *G. biloba*. First, the conceptually simple act of counting stomata and epidermal cells in order to calculate *SI* and SD_{ab} turns out to be difficult in practice. *G. biloba* has thin cuticle making it hard to prepare, and the ubiquitous papillae on the external surface of the lower cuticle make it difficult to distinguish the borders between adjacent epidermal cells. Smith et al. (2010) demonstrated that different preparation techniques on *G. biloba* could influence the *SI* counts, with acetate peels always producing lower values than macerated cuticle. Chen et al. (2001) found acetate peels of herbarium specimens inadequate for counting *SI* because outlines of epidermal cells were indistinct. Though non-destructive, neither acetate-peels, nor epifluorescence microscopy produce replicable results, as evidenced by our counts of specimens used by Royer (2003). Cell counts of *G. biloba* should be conducted on images that clearly show cell borders, which presently means chemically macerating specimens.

Second, previous studies that produced calibration curves for *G. biloba* did not photographically document stomatal counts and measurements (Beerling et al., 1998; Royer, 2003), nor were specimens retained. This important documentation has been done, at least in part, by some authors (Chen et al., 2001; Denk and Velitzelos, 2002; Quan et al., 2009; Bonis et al., 2010; Steinthorsdottir et al., 2011; Mays et al., 2015), though even in some recent papers raw count data were not reported and counted images were not archived (Mays et al., 2015). This makes it difficult to compare observations among investigators, which must be similar in order to use existing response curves and models.

Third, counting and measuring procedures must be standardized. All total diffusivity models use SD_{ab}, yet some follow the practice of Poole and Kürschner (1999) in which stomata and epidermal cells are counted only if they contact the left and upper sides of the counting box (Roth-Nebelsick et al., 2014), while others count any stoma or cell that enters the counting box (Franks et al., 2014). This can greatly affect SD_{ab} values (Poole and Kürschner, 1999), but the procedure is not always explicitly

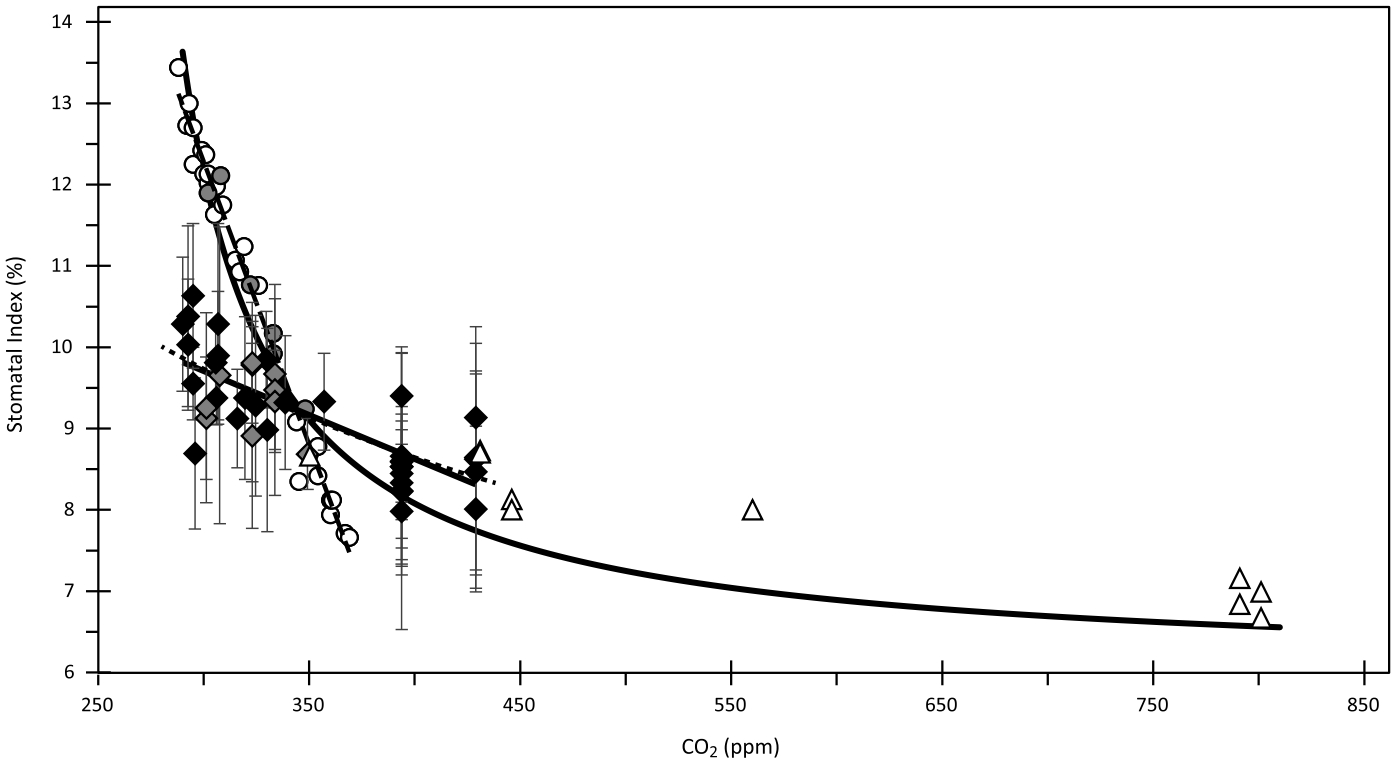

Fig. 3. Relationship between pCO_2 and stomatal index in *Ginkgo biloba*. Each symbol denotes the mean *SI* value for a single leaf. Diamonds – this study; gray fill – leaves from herbarium sheets sampled by Royer (2003) and recounted for this study; black fill – new samples from herbaria and living trees. Circles – data from Royer (2003); gray fill – leaves recounted for this study; white fill – leaves not recounted for this study. See Table 3 for comparison of our counts with those of Royer (2003). Triangles – data from plants grown in chambers (Royer, 2003). Error bars for Royer (2003) are not shown but were slightly larger than the symbols. Dashed lines – linear regressions through our data set and the herbarium data set of Royer (2003). Thick lines – power-curve regressions through our data set and the entire Royer (2003) data set. Regression statistics are reported in the text.

stated. Clearly, counting procedures must be the same for fossils and recent *G. biloba* if the response curve is to be used to estimate paleo-pCO_2.

4.2. Total diffusivity model

In the last few years a number of authors have developed total diffusivity models with the purpose of reconstructing paleo-pCO_2 from epidermal features without the need to construct a response curve (Grein et al., 2011; Franks et al., 2014; Roth-Nebelsick et al., 2014). Total diffusivity models are conceptually superior to the *SI* method because they use general physical and physiological properties of photosynthesis rather than relying on the specific relationship between pCO_2 and *SI* seen in an extant species, which may or may not accurately reflect the behavior of related extinct species.

The total diffusivity model recently described by Franks et al. (2014) reconstructs the pCO_2 of the atmosphere from the CO_2 assimilation rate of the leaf, the total conductance of CO_2 from the atmosphere to photosynthetic sites, and the ratio of CO_2 concentration inside the leaf to CO_2 concentration in the atmosphere. The total diffusivity of the leaf epidermis is calculated from measurements of stomatal density, pore length, and pore depth. The water use efficiency of the plant is estimated from its leaf-level carbon isotope discrimination.

When applied to our *G. biloba* sample set, the total diffusivity model produced a mean error about five times larger (mean predicted–observed value of ±109 ppm or ~30% of the estimate) than the regression models using *SI* and other stomatal measurements. Further, all but one of the pCO_2 estimates from the total diffusivity model was too high, and there is a strong pattern of increasing error with lower pCO_2. Thus, the total diffusivity model was less accurate and less precise than the statistical models in predicting pCO_2. The multiple regression analysis, which

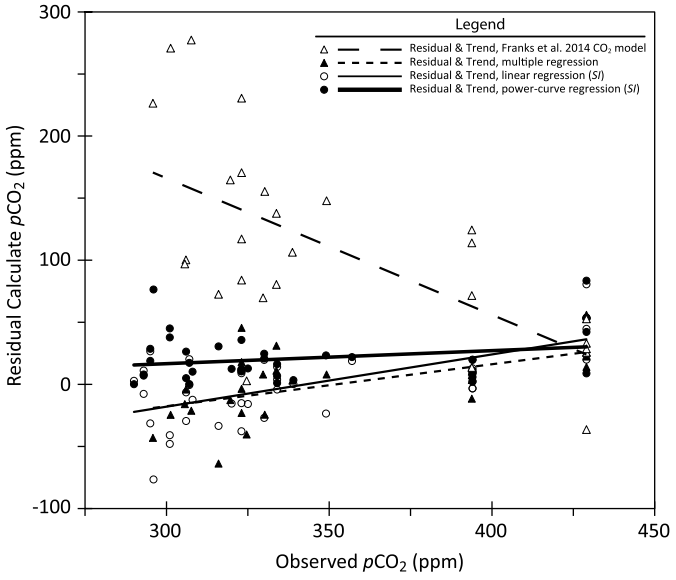

Fig. 4. Comparison of observed pCO_2 values with estimates made using three methods. Unfilled triangles: predicted–observed values, with predictions generated by the total diffusivity model of Franks et al. (2014). Filled triangles: residuals of pCO_2 estimates from multiple regression – $pCO_2 = 894.3 + [-8.01 \times 10^{-7}(SD_{ab})] + [5.86 \times 10^{6}(Gcl_{ab})] + [-2.14 \times 10^{7}(Gcw_{ab})] + [-10.46(\Delta^{13}C_{leaf})]$. Unfilled circles: residuals of pCO_2 estimates from linear regression [$pCO_2 = -53.66(SI) + 838.86$]. Filled circles: residuals of pCO_2 estimates from power curve regression [$pCO_2 = 9920.9(SI)^{-1.484}$]. Source of observed pCO_2 values given in text and supplementary material.

Table 3
pCO_2 estimates made using the power curve regression of *SI* against pCO_2 described in the text, and the total diffusivity model of Franks et al. (2014). For the six specimens used for this study and by Royer et al. (2001) counts were made from the same herbarium sheet, but not from the same leaf. Observed pCO_2 values come from sources identified in the text (also see Fig. S1 in Supplementary Material). Abbreviations: nd = no data.

Date collected	Sample No.	Leaf No.	*SI* count (Royer)	*SI* count (Barclay)	*SI* calculated CO_2	*SI* residual CO_2	Franks model calculated CO_2	Franks model residual CO_2	$\delta^{13}C$ atmosphere	Observed CO_2
5/24/1877	57 339	A	–	10.28	262.4	−27.7	nd	nd	−6.62	290
1888	57 342	A	–	10.38	256.6	−36.0	nd	nd	−6.65	293
1888	57 342	B	–	10.03	278.1	−14.5	nd	nd	−6.65	293
8/27/1896	57 363	A	–	10.63	242.6	−52.3	nd	nd	−6.67	295
8/27/1896	57 363	B	–	9.55	312.1	17.2	nd	nd	−6.67	295
10/1/1904	15 089	A	–	8.69	389.7	93.9	522.3	226.4	−6.69	296
8/1920	15 049	A	11.9	9.13	347.5	46.2	572.0	270.7	−6.73	301
8/1920	15 049	B	–	9.26	336.1	34.8	nd	nd	−6.73	301
5/29/1928	3804	A	–	9.81	293.0	−12.6	402.6	97.0	−6.75	306
10/10/1931	15 088	A	–	9.38	326.0	20.0	406.2	100.2	−6.76	306
10/26/1936	227 512	A	–	10.29	262.1	−44.6	nd	nd	−6.77	307
10/26/1936	227 512	B		9.90	287.1	−19.6	nd	nd	−6.77	307
11/29/1942	3805	A	12.11	9.66	304.3	−3.3	584.9	277.3	−6.79	308
11/12/1959	15 101	A	–	9.12	347.7	31.7	388.5	72.5	−7.05	316
7/22/1964	15 085	A	–	9.38	326.1	6.4	484.3	164.7	−7.17	320
6/25/1968	15 024	A	–	9.42	329.7	6.7	440.1	117.1	−7.26	323
8/22/1968	15 025	A	–	9.78	295.0	−28.0	493.5	170.5	−7.26	323
10/9/1968	15 030	A	–	9.81	293.4	−29.7	407.1	84.0	−7.26	323
10/15/1968	3806	A	10.77	8.91	367.7	44.7	553.5	230.5	−7.26	323
10/23/1969	15 064	A	–	9.28	334.0	9.4	327.5	2.9	−7.29	325
7/19/1973	15 073	A	–	9.85	290.6	−39.1	399.4	69.7	−7.38	330
7/17/1974	15 096	A	–	8.98	360.5	30.3	485.6	155.4	−7.40	330
8/26/1977	3809	A	9.92	9.33	329.5	−4.3	414.2	80.4	−7.47	334
10/9/1977	3807	A	10.17	9.67	303.2	−30.6	471.4	137.7	−7.47	334
10/9/1977	3807	B	–	9.48	317.9	−15.9	nd	nd	−7.47	334
7/1/1980	15 069	A	–	9.32	330.8	−7.9	445.1	106.4	−7.58	339
6/30/1987	3808	A	9.24	8.69	390.3	41.1	497.1	147.9	−7.71	349
11/27/1993	15 055	A	–	9.33	329.8	−27.3	nd	nd	−7.85	357
9/27/2012	RSB1273A	A	–	8.45	390.0	−3.8	nd	nd	−8.37	394
9/27/2012	RSB1274A	A	–	8.53	407.1	13.3	507.7	113.9	−8.37	394
9/27/2012	RSB1274B	B	–	8.23	442.6	48.8	518.2	124.3	−8.37	394
9/27/2012	RSB1274C	C	–	8.33	430.3	36.5	465.3	71.5	−8.37	394
9/27/2012	RSB1274D	D	–	8.66	393.0	−0.8	407.3	13.5	−8.37	394
9/27/2012	RSB1274E	E	–	8.23	443.5	49.7	nd	nd	−8.37	394
10/8/2013	RSB1343A	A	–	8.64	394.8	−34.2	454.8	25.8	−8.37	429
10/8/2013	RSB1343B	B	–	8.01	472.3	43.3	462.1	33.1	−8.37	429
10/8/2013	RSB1343C	C	–	8.63	396.8	−32.2	481.8	52.8	−8.37	429
10/8/2013	RSB1343D	D	–	9.14	346.6	−82.4	457.6	28.6	−8.37	429
10/8/2013	RSB1343E	E	–	8.47	414.6	−14.4	392.5	−36.5	−8.37	429
2013	RSB1432_Gb1A	R17	–	8.87	371.2	−8.8	nd	nd	na	380
2013	RSB1433_Gb1A	R33	–	13.06	149.4	−230.6	nd	nd	na	380
2013	RSB1435_Gb2A	R50	–	8.99	360.0	−20.0	nd	nd	na	380
2013	RSB1434_Gb2A	R60	–	7.90	487.7	107.7	nd	nd	na	380
2013	RSB1436_Gb3A	R10	–	8.25	440.8	60.8	nd	nd	na	380
2013	RSB1437_Gb3A	R20	–	9.02	356.9	−23.1	nd	nd	na	380
2013	RSB1438_Gb1D	R21	–	9.24	337.6	−1162.5	nd	nd	na	1500
2013	RSB1439_Gb1D	R50	–	12.30	172.1	−1327.9	nd	nd	na	1500
2013	RSB1441_Gb2D	R33	–	9.96	283.0	−1217.0	nd	nd	na	1500
2013	RSB1440_Gb2D	R57	–	13.48	138.7	−1361.3	nd	nd	na	1500
2013	RSB1442_Gb3D	17	–	9.61	307.3	−1192.7	nd	nd	na	1500
2013	RSB1443_Gb3D	12	–	8.22	444.0	−1056.0	nd	nd	na	1500

uses the same four variables we measured for the total diffusion model, produced pCO_2 estimates with far less error (mean residual ±21.4 ppm or 6% of the estimate) and with less systematic bias. This suggests that there is information about pCO_2 in some of the variables used in the total diffusivity model (SD_{ab} and Gcw_{ab}), but that other variables, or the relationships among them stipulated in the model, are obscuring this information. We directly measured four of the required variables on our *G. biloba* samples: Gcl_{ab}, Gcw_{ab}, SD_{ab}, and $\Delta^{13}C_{leaf}$. For the other required variables, we used the same values used by Franks et al. (2014) for photosynthetic rate (A_0), boundary layer conductance (g_b), scaling of maximum conductance to CO_2 (g_{cop}), and scaling from photosynthetic rate to mesophyll conductance to CO_2 (g_m). It could be that better estimates of these variables for living *G. biloba* would improve the ability of the total diffusivity model to estimate pCO_2.

4.3. New stomatal index response curve for Ginkgo biloba

Until further improvements are made to total diffusivity models, it appears that stomatal index remains the best available proxy for estimating paleo-pCO_2, and it has also been widely applied. With the addition of the data presented here, there are now three separate curves representing the response of *G. biloba SI* to changes in pCO_2. The response curve presented by Retallack (2001) is based on 8 data points from the historical anthropogenic rise in pCO_2, with one additional point at higher than ambient pCO_2 derived from an experiment by Beerling et al. (1998). This curve of Retallack (2001) has not been widely used in subsequent papers reconstructing paleo-pCO_2 so we do not discuss it further.

The response curve published by Royer et al. (2001) has, in contrast, been applied widely in estimating paleo-pCO_2 and has been modified in subsequent publications (Wynn, 2003; Beerling et al., 2009). This curve has been used by 48 publications either

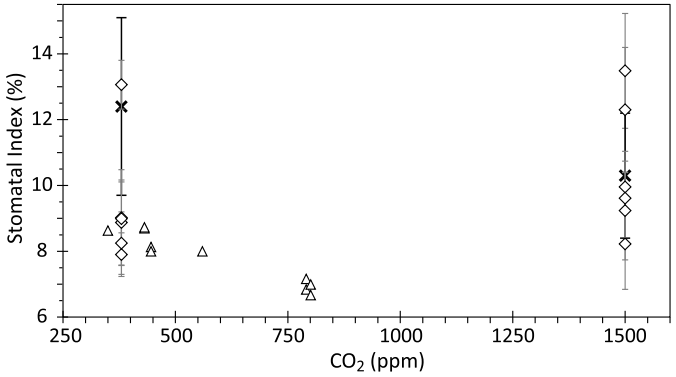

Fig. 5. Stomatal index values of *Ginkgo biloba* plants grown in environmental chambers. Diamonds – our counts of leaves grown in the experiment of Haworth et al. (2013). Two leaves were counted for each of three plants grown under 380 ppm and 1500 ppm pCO_2. Error bars are 1σ. Crosses – mean stomatal index values for other leaves from the same plants reported by Haworth et al. (2013). Triangles – mean values for chamber-grown plants from Royer (2003). Original error bars (s.e.m.) were about the size of the symbols.

to estimate paleo-pCO_2 from fossil *Ginkgo* (or related taxa) or by authors comparing estimates from other proxies with those made using *G. biloba*. These 48 publications have received 3377 citations (Google Scholar, accessed 10th Jan. 2015), a strong indicator of how significantly the *G. biloba* calibration of Royer et al. (2001) has affected our understanding of paleo-pCO_2. Most of the data for this curve came from herbarium leaves that were collected between 1856 and 2000 (39 specimens; pCO_2 range 288–369 ppm), but leaves of experimental plants (Beerling et al., 1998; Royer, 2003) were used to determine the response of *SI* to pCO_2 above 369 ppm (Fig. 3, triangles). Royer et al. (2001) used a power function to describe the combined data set (Wynn, 2003), but the portion of the curve measured on herbarium leaves alone is quite linear, with a steep slope (−0.07), and a high correlation coefficient (Fig. 3; $r^2 = 0.98$). The overall response curve inflects sharply at ∼380 ppm, which corresponds to the shift from herbarium leaves (studied with epifluorescent illumination) to those grown under experimental conditions (chemically macerated). The original *G. biloba* response curve was reinterpreted in many later publications using new statistical approaches (Beerling et al., 2009), but the primary *SI* data set from *G. biloba* remained unmodified.

Our data set includes leaves from six herbarium sheets originally sampled for the response curve of Royer et al. (2001). In all cases, our counts were lower than the original counts and the magnitude of the difference increased with increasing *SI* (Table 3). Miscounting stomata is unlikely because they are quite distinctive, and the discrepancy is also unlikely to result from heterogeneity in *SI* within leaves, since we have shown this is insignificant. We suggest that the difference between Royer's counts and ours reflects the difficulty of differentiating and counting epidermal cells using epifluorescence. Missing some epidermal cell borders would increase *SI* values and the effect would be greater with higher *SI* values.

The *SI* response curve generated from our data has greater scatter and a much shallower slope between 280 and 380 ppm than that described by Royer et al. (2001). The addition of data from leaves from outdoor trees grown under pCO_2 of 430 ppm continues the more linear trend we observe at lower pCO_2 (Fig. 3). The strength of the correlation we observed in *G. biloba* is similar to *SI* calibration datasets established for other species of gymnosperms (Kouwenberg et al., 2003) and angiosperms (Wagner et al., 1999; Kürschner et al., 2008).

The new *G. biloba* calibration has a shallow slope (−0.011 in a linear model) compared with other species. The only other comparably shallow slope for a calibration dataset is from *Hypdaphnis zenkeri* (Barclay et al., 2010), the basal taxon of the Lauraceae family, with a slope of −0.025. The typical range of slopes for angiosperm species is between −0.055 and −0.065 (Wagner et al., 1996, 2005; Kürschner et al., 2008). The slope of a linear fit to the herbarium specimens of *G. biloba* sampled by Royer et al. (2001) is −0.070, steeper than observed in any other species.

The shallow slope we observe in the *SI* response curve of *G. biloba* may relate to several unusual features of *Ginkgo*. Unlike most extant gymnosperms, which have stomata in rows, *G. biloba* has stomata that are randomly dispersed between parallel veins. This makes the *SI* of *Ginkgo* hard to compare with other gymnosperms, whose *SI* is calculated from the number of stomata per unit of needle length rather than the number per epidermal cell (McElwain et al., 2002; Kouwenberg et al., 2003). The shallow slope in *G. biloba* could also reflect the evolution of its lineage during the extended period of high pCO_2 in the late Mesozoic and early Cenozoic and the small amount of morphological change that has occurred since. Finally, *G. biloba* exerts only passive metabolic stomatal control; guard cell turgor reflects plant water status (Brodribb and McAdam, 2011). The inability of *G. biloba* to control stomatal aperture size through active ion transport in the guard cells (Brodribb and McAdam, 2011) may mean it can only respond to changes in pCO_2 through changes in *SI*.

4.4. SI response in Ginkgo biloba above 430 ppm pCO_2

The response of *SI* to pCO_2 above 430 ppm is most important for inferring pCO_2 during the Late Cretaceous and Paleogene, when pCO_2 is thought to have been high, but few data are available at elevated pCO_2 to constrain the calibration, and *SI* of *G. biloba* grown at high pCO_2 is highly variable. Experimental work shows that the *G. biloba* response to elevated pCO_2 doesn't begin to asymptote until 24 months (Overdieck and Strassemeyer, 2005), which may explain the high *SI* variance in the specimens of Haworth et al. (2013). An incomplete anatomical adjustment to high pCO_2 may also be suggested by the high proportion of deformed stomata and guard cells we observed in Haworth et al.'s plants. It is clear that more and better experimental data are needed to define the shape of the *SI* response curve for *G. biloba* at pCO_2 greater than 430 ppm.

We have not included chamber-grown plants in the *SI* response curve presented here because we were unable to restudy samples from Beerling et al. (1998) and Royer et al. (2001), and because we observed abnormal stomata and high variance in *SI* among the leaves grown under elevated pCO_2 by Haworth et al. (2013). However, if we extrapolate the power curve developed from our data on herbarium sheets and living plants to pCO_2 levels beyond 430 ppm, the curve passes near the *SI* values that Royer et al. (2001) reported for plants grown at 445 ppm, 550 ppm, and 800 ppm pCO_2 (Fig. 3). Although better definition of the *G. biloba* response curve at pCO_2 above 430 ppm awaits new data, it is worth exploring the effect of our response curve on previous estimates of pCO_2 for the Late Cretaceous and Cenozoic.

4.5. Effect of the new Ginkgo biloba calibration on paleo-pCO_2 estimates

We recalculated paleo-pCO_2 estimates for the Late Cretaceous and Cenozoic, compiling all published estimates of pCO_2 based upon specimens originally identified as *G. adiantoides* (Table 4). These are mostly from North America, with a few specimens from China and Europe providing greater temporal coverage. We used the originally reported *SI* values from fossils and the power regression that best fits our dataset [$pCO_2 = 9920.9(SI)^{-1.484}$] to make new estimates of paleo-pCO_2 (filled circles in Fig. 7). We did not

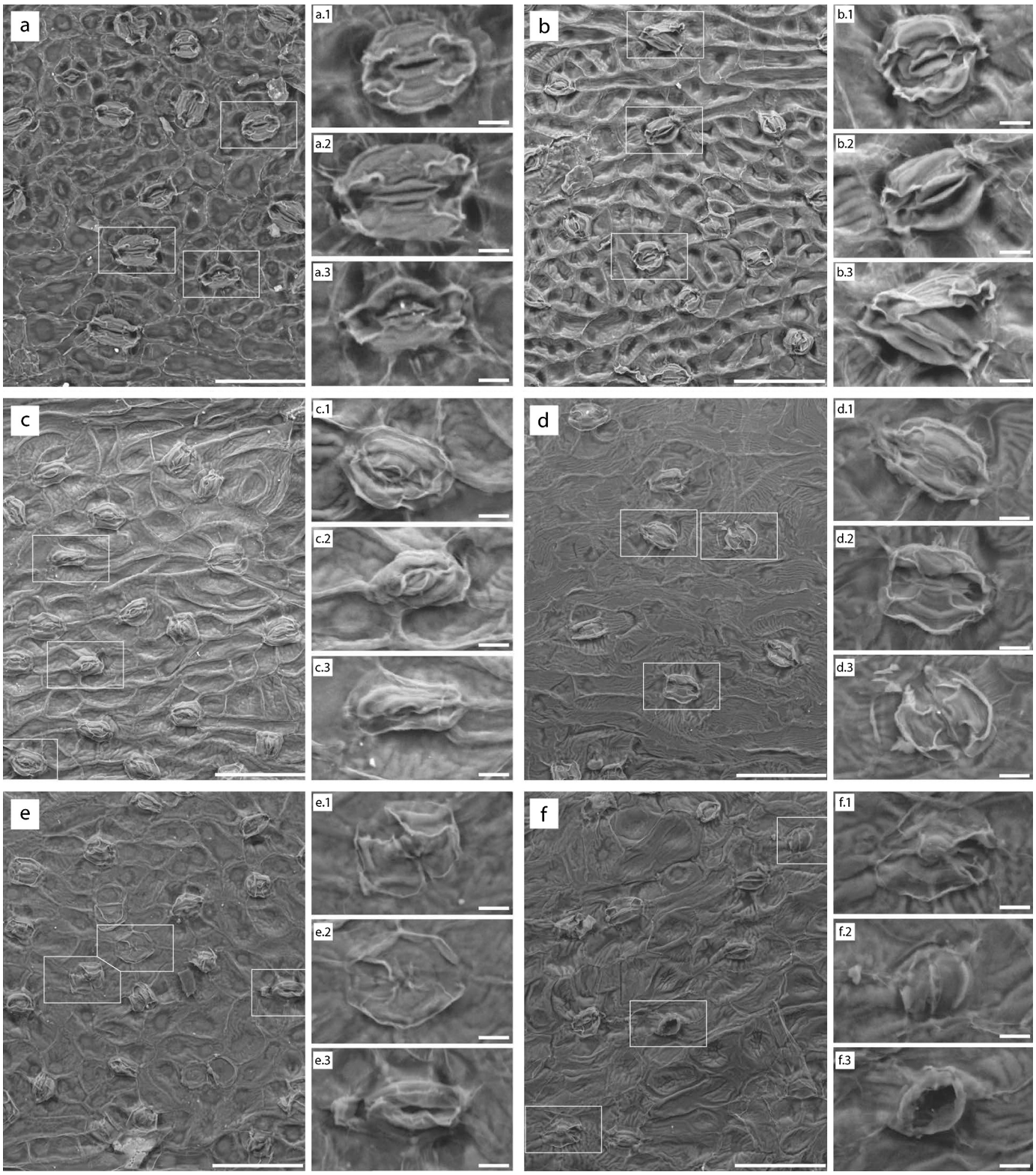

Fig. 6. SEM images of *Ginkgo biloba* leaves showing the range of development of stomata. (a–b) Trees from Blandy Experimental Farm, Virginia Arboretum, near Boyce, VA. (a) Collected from live tree in 2012 (395 ppm pCO_2). (b) Herbarium sheet collected in 1977 (334 ppm pCO_2). (c–f) Plants grown for 18 months in controlled environmental conditions in the Program for Experimental Atmospheres and Climate (Péac) at University College Dublin, Ireland (Haworth et al., 2013). (c–d) Plants grown at pCO_2 of 380 ppm. (e–f) Plants grown at pCO_2 of 1500 ppm. Inset photos are 300% enlargements of portions of the same image displayed to the left. Note incomplete development of pores and guard cells forming stomata in c–f. All scale bars are 100 µm.

correct published age estimates. We compare these new pCO_2 estimates with global surface temperature estimates derived from $\delta^{18}O$ values of benthic foraminifera (Hansen et al., 2013).

The shallower slope of our new regression has the effect of reducing some pCO_2 estimates ($n = 25$) and elevating others ($n = 16$; ΔCO_2 in Table 4). Some of the new estimates of pCO_2 from the

Table 4
Revised estimates of paleo-pCO_2 using the power curve regression presented in this paper. Stomatal index counts and sample ages of *Ginkgo adiantoides* leaves are from the cited source and were not reevaluated.

Sample number or publication	Region/state	Country	Source *SI* count	Stomatal index (*SI*)	Old CO_2 estimate (ppm)	Revised CO_2 estimate (ppm)	Δ CO_2 (ppm)	Stage/epoch	Age (Ma)[a]
Florin, 1937, Tralau, 1968	Klärbecken	GER	Retallack, 2001	8.1 ± 1.9	521	460	−61	Pliocene	4.0 ± 2
Szafer, 1961	Stare Gliwice	POL	Retallack, 2001	9.6 ± 0.8	310	309	−1	Miocene	ca. 6.3
Lancucka-Środoniova, 1966	Klaj	POL	Retallack, 2001	8.2 ± 1.5	485	447	−38	Miocene	ca. 7.8
GA (MN6)[b]	Zukunft-W	GER	Kürschner et al., 2008	14.64 ± 1.43	280	114	−166	Miocene	13.9 ± 0.4
HB2/1 – Horni Briza[b]	W. Bohemia	CZE	Kürschner et al., 2008	7.68 ± 0.46	438	521	+83	Miocene	15.7 ± 0.7
HB2/2 – Horni Briza[b]	W. Bohemia	CZE	Kürschner et al., 2008	7.86 ± 0.75	420	494	+74	Miocene	15.7 ± 0.7
U. Cedarville Fm.; 49Camp	Nevada	USA	Retallack, 2002	7.6 ± 1.3	440	535	+95	Miocene	15.8 ± 0.02
Juliaetta (P6)	Idaho	USA	Royer, 2003	8.14	396	430	+34	Miocene	16.5
Smith et al., 2010, Mean	Alberta	CAN	Smith et al., 2010	5.8	600	1178	+578	Eocene	50.61 ± 0.16
LJH9915	Wyoming	USA	Royer, 2003	9.38	342	326	−16	Eocene	53.4
SLWH	Wyoming	USA	Royer, 2003	10.22	323	266	−57	Eocene	53.5
SLWLB	Wyoming	USA	Royer, 2003	9.29	345	333	−12	Eocene	53.9
SLW9915	Wyoming	USA	Royer, 2003	8.83	360	376	+16	Eocene	54.8
SLW9812	Wyoming	USA	Royer, 2003	8.53	373	407	+34	Eocene	55.1
SLW9715	Wyoming	USA	Royer, 2003	8.23	390	443	+53	Paleocene	55.3
SLW9050	Wyoming	USA	Royer, 2003	12.18	300	176	−124	Paleocene	55.3
SLW9936	Wyoming	USA	Royer, 2003	11.77	303	191	−112	Paleocene	55.3
SLW8612	Wyoming	USA	Royer, 2003	12.41	298	169	−129	Paleocene	55.3
SLW9434	Wyoming	USA	Royer, 2003	12.23	299	175	−124	Paleocene	55.4
SLW9411	Wyoming	USA	Royer, 2003	11.5	306	202	−104	Paleocene	55.6
SLW9155	Wyoming	USA	Royer, 2003	11.21	309	214	−95	Paleocene	55.7
LJH72141-1	Wyoming	USA	Royer, 2003	10.63	317	243	−74	Paleocene	55.8
SLW991	Wyoming	USA	Royer, 2003	10.97	312	226	−86	Paleocene	55.9
SLW992	Wyoming	USA	Royer, 2003	10.8	314	234	−80	Paleocene	55.9
SLW993	Wyoming	USA	Royer, 2003	11.43	307	205	−102	Paleocene	55.9
LJH7132	Wyoming	USA	Royer, 2003	8.75	363	384	+21	Paleocene	56.4
SLW0025	Wyoming	USA	Royer, 2003	9.01	353	350	−3	Paleocene	57.3
Burbank	Alberta	CAN	Royer, 2003	7.55	451	543	+92	Paleocene	58.5
Joffre Bridge	Alberta	CAN	Royer, 2003	7.96	409	479	+70	Paleocene	58.5
DMNH2644	Wyoming	USA	Royer, 2003	10.93	313	227	−86	Paleocene	61.0
Collinson et al., 1998	Wyoming	USA	Retallack, 2001	6.7 ± 0.4	1350	719	−631	Paleocene	63.0 ± 2
Manum, 1966[c]	Wyoming	USA	Retallack, 2001	4.1 ± 0.2	4510	2285	−2225	Paleocene	64.0 ± 2
DMNH2360	Colorado	USA	Royer, 2003	9.9	329	287	−42	Paleocene	64.1
LJH7423	Wyoming	USA	Royer, 2003	9.48	339	316	−23	Paleocene	64.5
LJH7659	Wyoming	USA	Royer, 2003	9.32	344	331	−13	Paleocene	64.5
DMNH 1489	North Dakota	USA	Beerling et al., 2002	8.4 ± 0.3	361	423	+62	Maastrichtian	65.4
DMNH 566	North Dakota	USA	Royer, 2003	8.32	385	432	+47	Maastrichtian	65.5
DMNH 572	North Dakota	USA	Beerling et al., 2002	7.1 ± 0.3	527	628	+101	Maastrichtian	65.8
DMNH 571	North Dakota	USA	Beerling et al., 2002	7.0 ± 0.5	554	648	+94	Maastrichtian	65.9
Mösle et al., 1998	North Dakota	USA	Retallack, 2001	8.1 ± 0.7	521	460	−61	Maastrichtian	66.0 ± 2
Taipinglinchang Fm. Mean	Heilongjiang	China	Quan et al., 2009	6.92	559	667	+108	Campanian	77.8 ± 4.2

[a] The age presented is the published age and has not been corrected. The period/epoch remains appropriate. Fossils originally described as: [b]*Ginkgo biloba*, [c]*Ginkgo wyomingensis*.

new calibration are surprisingly low, including one from the early Paleocene (227 ppm) and ten from the late Paleocene (169–243 ppm). There is evidence for high global temperatures and an absence of continental glaciers during these intervals (Fig. 7). Another unexpectedly low estimate (114 ppm) comes from the Miocene of Germany (Kürschner et al., 2008). This sample coincides with the Mi 3/4 transition and expansion of the East Antarctic ice sheet, but the estimate is below the ~180 ppm value typical of maximum glacial advance in the Quaternary (Siegenthaler et al., 2005).

The new calibration increases 16 estimates of pCO_2 by an average of 87 ppm. Some of these now fit better with other proxy data from the Cenozoic (Beerling and Royer, 2011). The new calibration also permits pCO_2 estimates for *SI* values that fell below the earlier response curve and therefore had undefined pCO_2. The early Eocene Falkland site (Smith et al., 2010) now provides a paleo-pCO_2 estimate of 843 ppm, fitting for its position in the Early Eocene Climate Optimum, one of the warmest intervals of the Cenozoic (Hansen et al., 2013).

4.6. The effect of fossil preservation on paleo-pCO_2 estimates

High pCO_2 estimates published by Retallack (2001) decrease significantly with the new response curve, but they remain among the highest estimates for the Cenozoic when we apply our new calibration curve (Fig. 7; Table 4). For these two samples we reinvestigated the original images and specimens from which *SI* values were obtained. Retallack (2001) counted an image of *G. wyomingensis* (synonymous with *G. adiantoides*) cuticle from Manum (1966; Fig. S4), making a pCO_2 estimate of 4510 ppm at 64Ma based upon an *SI* of 4.1 ± 0.2 (from 517 cells and 23 stomata). Re-examining an original reprint of Manum's paper, we found it difficult to properly identify stomata, and impossible to discern epidermal cell boundaries (Fig. S4). As a further check, we examined the specimen figured by Manum (Yale Peabody Museum 45127), the type of *G. wyomingensis*. Stomata were clearly visible on the separated lower surface, and in some areas epidermal cells could be differentiated, but never over an area large enough to provide even one stomatal index count (×400; 250 × 250 μm box). The second highest pCO_2 estimate for the Paleogene (1350 ppm at 63 Ma

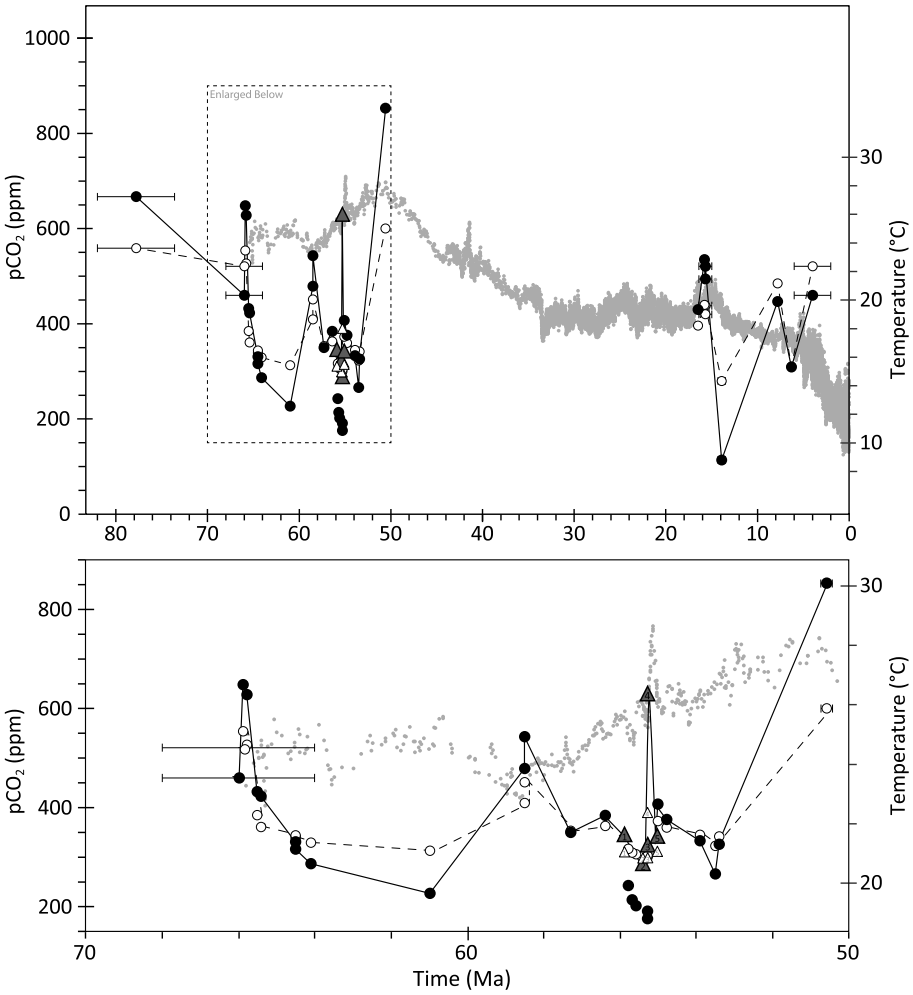

Fig. 7. Estimates of pCO_2 for the past 80 Ma from *SI* counts on fossil leaves of *Ginkgo adiantoides*. Circles use published *SI* values: open circles and dashed line use regression of Royer (2003); filled circles and solid line use power-curve regression from this paper. Triangles are estimates from reinvestigated fossil material: open triangles used published *SI* values and the regression of Royer (2003); filled triangles use new *SI* counts with the power-curve regression described in the text. Temporal error bars from original publication where available (Table 4). Global temperature curve from Hansen et al. (2013).

from an *SI* of 6.7 ± 0.4; 723 cells and 50 stomata reported by Retallack, 2001) was derived from a sample figured by Collinson et al. (1998; Fig. S5). In this figure, cell boundaries are well defined but stomata are small and indistinct on the ×50 image. Because neither sample provides sufficient detail to make an accurate *SI* counts we reject these two paleo-pCO_2 estimates.

More generally, we suspect that poor cuticle preservation reduces the quality of many paleo-pCO_2 estimates. We re-examined 19 specimens of *G. adiantoides* from five previously reported Paleogene localities (Royer, 2003), using only the specimens with the best preservation. Four of our new *SI* counts were lower than the originals (Tables S4–S5), but for one site the new counts were higher. *SI* counts probably differ between observers because most fossils from these localities are only moderately well preserved, making the recognition of cell boundaries difficult. Using both the new *SI* counts for these fossils and the revised response curve increased paleo-pCO_2 estimates by an average of 54 ppm (filled triangles in Fig. 7).

Even though we have improved the *SI*-pCO_2 response curve for *G. biloba* and the *SI* counts on some fossil *G. adiantoides*, this does not uniformly elevate paleo-pCO_2 estimates for the Late Cretaceous and Cenozoic. Also, because the *SI* values of re-examined fossil specimens are not predictably different, it is not possible to apply an offset to remedy all paleo-pCO_2 estimates. The overall pattern of change in paleo-pCO_2 through the last 80 million years shows limited correspondence with changes in temperature. It is especially surprising that paleo-pCO_2 estimates for the greenhouse world of the early Cenozoic are not consistently higher than those for the icehouse world of the late Cenozoic. A rigorous re-evaluation of the quality of the *SI* counts is required to fully understand the discrepancy between the modest pCO_2 estimates from *SI* and the high pCO_2 needed to produce greenhouse temperatures in many climate models (Lunt et al., 2012). New global climate models that utilize lower levels of cloud condensation nuclei may provide a partial solution, as they are the best at matching the shallow latitudinal temperature gradients suggested by proxy data during greenhouse intervals (Sagoo et al., 2013; Upchurch et al., 2015), yet require only modest levels of pCO_2, more consistent with our revised *SI*-based paleo-pCO_2 estimates.

5. Conclusions

Earlier studies of *SI* in *G. biloba* did not prepare and count stomata in a consistent manner, nor were stomatal and epidermal cell counts fully documented. We do not consider previously published *SI* response curves to be reliable and recommend they no longer be used to reconstruct paleo-pCO_2. A new *SI* response curve for *G. biloba* developed from plants that grew between 290–430 ppm pCO_2 shows a statistically significant negative relationship with a

much shallower slope than previous response curves, and is less strongly curved. Testing of the recently developed total diffusivity model for CO_2 shows that it performs less well in predicting pCO_2 for *G. biloba* than *SI* methods.

Stomatal response of *G. biloba* to pCO_2 levels above 430 ppm is still poorly constrained. Specimens from a previous growth chamber experiment show malformed stomata, suggesting incomplete phenotypic adaptation to elevated pCO_2. No consistent relationship is seen between *SI* and pCO_2 in high CO_2 experimental plants, therefore estimates of paleo-pCO_2 higher than 430 ppm should be regarded with caution.

Estimates of Cretaceous and Cenozoic pCO_2 derived by applying the new *Ginkgo SI* response curve to fossil leaves of *G. adiantoides* show a limited correlation between reconstructed paleo-pCO_2 values and global temperature estimates during the last 80 Ma. Further, our paleo-pCO_2 estimates for the late Cretaceous and Paleogene remain lower than most climate models require to produce globally warm climate. This suggests that either the estimates of paleo-pCO_2 are still faulty, global surface paleotemperature estimates are problematic, and/or that the relation between global temperature and atmospheric concentration of pCO_2 over geological time is not what we expect. We think estimates of paleo-pCO_2 from *Ginkgo SI* can be improved by new studies of *G. biloba* grown in elevated pCO_2 longer than two years, by higher quality counts of fossil *Ginkgo*, and by improved models of stomatal function.

Acknowledgements

Robert Webster and Joe Kirkbride provided access and permission to sample herbarium specimens at the National Arboretum Herbarium (NA). Rusty Russell provided permission and Deborah Bell provided access to sample in the National Museum of Natural History Herbarium (US – Smithsonian Institution). Shusheng Hu facilitated the specimen loan from the Yale Peabody Museum. Emily Martin helped sample living trees in the "Ginkgo Grove" at the Blandy Experimental Farm near Boyce, VA. Access and sampling permission at Blandy were provided by Kyle Haynes, Research Assistant Professor in the Department of Environmental Sciences at the University of Virginia. We thank Jennifer McElwain of University College Dublin for providing *Ginkgo biloba* leaves from the experiment of Haworth et al. (2013). NMNH volunteer Sal Bosco prepared and mounted most of the *Ginkgo* specimens. We thank Odile Madden from the Museum Conservation Institute (Smithsonian Institution) for suggesting imaging *Ginkgo* specimens with an environmental SEM. Volunteer Pam Hamilton spent hundreds of hours taking SEM images at NMNH and also helped test the stomatal measurement approaches; without her efforts this project would not have been completed. Intern Rebecca Blader (Paleobiology) helped initiate the SEM imaging project. Scott Whittaker and Caitlin Baker provided training in the operation of the Zeiss environmental SEM at the National Museum of Natural History. International summer interns Nicolás Pérez (Colombia) and Rolf Svenning (Denmark) in the Paleobiology Department at NMNH were pivotal in preparing samples for carbon isotope measurement at the Isotope Ratio Mass Spectrometry lab of the Museum Conservation Institute, under the direction of Christine France. Funding for RSB comes from a Peter Buck Postdoctoral Fellowship at the Smithsonian's National Museum of Natural History in Washington, D.C.

Appendix A. Supplementary material

Supplementary material related to this article can be found online at http://dx.doi.org/10.1016/j.epsl.2016.01.012.

References

Barclay, R.S., McElwain, J.C., Dilcher, D.L., Sageman, B.B., 2007. The cuticle database: developing an interactive tool for taxonomic and paleoenvironmental study of the fossil cuticle record. In: Jarzen, D.M., Manchester, S.R., Retallack, G.J., Jarzen, S.A. (Eds.), Advances in Angiosperm Paleobotany and Paleoclimatic Reconstruction – Contributions Honoring David L. Dilcher and Jack A. Wolfe. In: Courier Forschungsinstitut Senckenberg, vol. 258, pp. 39–55.

Barclay, R.S., McElwain, J.C., Sageman, B.B., 2010. Carbon sequestration activated by a volcanic CO_2 pulse during Ocean Anoxic Event 2. Nat. Geosci. 3, 205–208.

Barclay, R.S., Wilf, P., Dilcher, D.L., McElwain, J.C., 2012. The cuticle database project. The Earth and Environmental Systems Institute of Pennsylvania State University, http://cuticledb.eesi.psu.edu/, version 1.1.

Beerling, D.J., Lomax, B.H., Royer, D.L., Upchurch, G.R., Kump, L.R., 2002. An atmospheric pCO_2 reconstruction across the Cretaceous–Tertiary boundary from leaf megafossils. Proc. Natl. Acad. Sci. USA 99, 7836–7840.

Beerling, D.J., 2014. Personal communication. Department of Animal and Plant Sciences, University of Sheffield, UK.

Beerling, D.J., Fox, A., Anderson, C.W., 2009. Quantitative uncertainty analyses of ancient atmospheric CO_2 estimates from fossil leaves. Am. J. Sci. 309, 775–787.

Beerling, D.J., Kelly, C.K., 1997. Stomatal density responses of temperate woodland plants over the past seven decades of CO_2 increase: a comparison of Salisbury (1927) with contemporary data. Am. J. Bot. 84, 1572–1583.

Beerling, D.J., McElwain, J.C., Osborne, C.P., 1998. Stomatal responses of the 'living fossil' *Ginkgo biloba* L. to changes in atmospheric CO_2 concentrations. J. Exp. Bot. 49, 1603–1607.

Beerling, D.J., Royer, D.L., 2011. Convergent cenozoic CO_2 history. Nat. Geosci. 4, 419–420.

Bonis, N.R., van Konijnenburg-van Cittert, J.H.A., Kürschner, W.M., 2010. Changing CO_2 conditions during the end-Triassic inferred from stomatal frequency analysis on *Lepidopteris ottonis* (Goeppert) Schimper and *Ginkgoites taeniatus* (Braun) Harris. Palaeogeogr. Palaeoclimatol. Palaeoecol. 295, 146–161.

Brodribb, T.J., McAdam, S.A.M., 2011. Passive origins of stomatal control in vascular plants. Science 331, 582–585.

Chen, L.Q., Li, C.S., Chaloner, W.G., Beerling, D.J., Sun, Q.G., Collinson, M.E., Mitchell, P.L., 2001. Assessing the potential for the stomatal characters of extant and fossil *Ginkgo* leaves to signal atmospheric CO_2 change. Am. J. Bot. 88, 1309–1315.

Collinson, M.E., Mosle, B., Finch, P., Scott, A.C., Wilson, R., 1998. The preservation of plant cuticle in the fossil record: a chemical and microscopical investigation. Anc. Biomol. 2, 251–265.

Denk, T., Velitzelos, D., 2002. First evidence of epidermal structures of *Ginkgo* from the Mediterranean Tertiary. Rev. Palaeobot. Palynol. 120.

Florin, R., 1937. Die fossile Ginkgophyten von Franz-Joseph-Land, nebst Erörterungen über vermeintliche Cordaitales mesozoischen Alters. Part 2. Allgemeiner Teil. Palaeontographica B 82, 1–72.

Franks, P.J., Royer, D.L., Beerling, D.J., Van de Water, P.K., Cantrill, D.J., Barbour, M.M., Berry, J.A., 2014. New constraints on atmospheric CO_2 concentration for the Phanerozoic. Geophys. Res. Lett. 41, 1–10.

Friedli, H., Lötscher, H., Oeschger, H., Siegenthaler, U., Stauffer, B., 1986. Ice core record of $^{13}C/^{12}C$ ratio of atmospheric CO_2 in the past two centuries. Nature 324, 237–238.

Grein, M., Konrad, W., Wilde, V., Utescher, T., Roth-Nebelsick, A., 2011. Reconstruction of atmospheric CO_2 during the early middle Eocene by application of a gas exchange model to fossil plants from the Messel Formation, Germany. Palaeogeogr. Palaeoclimatol. Palaeoecol. 309, 383–391.

Hansen, J., Sato, M., Russell, G., Kharecha, P., 2013. Climate sensitivity, sea level and atmospheric carbon dioxide. Philos. Trans. R. Soc. A 371, 20120294.

Haworth, M., Elliott-Kingston, C., McElwain, J.C., 2013. Co-ordination of physiological and morphological responses of stomata to elevated $[CO_2]$ in vascular plants. Oecologia 171, 71–82.

Keeling, C.D., Piper, S.C., Bacastow, R.B., Wahlen, M., Whorf, T.P., Heimann, M., Meijer, H.A., 2005. Atmospheric CO_2 and $^{13}CO_2$ exchange with the terrestrial biosphere and oceans from 1978 to 2000: observations and carbon cycle implications. In: Ehleringer, J.R., Cerling, T.E., Dearing, M.D. (Eds.), A History of Atmospheric CO_2 and Its Effects on Plants, Animals, and Ecosystems. Springer-Verlag, New York, pp. 83–113.

Kouwenberg, L.L.R., McElwain, J.C., Kurschner, W.M., Wagner, F., Beerling, D.J., Mayle, F.E., Visscher, H., 2003. Stomatal frequency adjustment of four conifer species to historical changes in atmospheric CO_2. Am. J. Bot. 90, 610–619.

Kürschner, W.M., Kvaček, Z., Dilcher, D.L., 2008. The impact of Miocene atmospheric carbon dioxide fluctuations on climate and the evolution of terrestrial ecosystems. Proc. Natl. Acad. Sci. USA 105, 449–453.

Kürschner, W.M., van der Burgh, J., Visscher, H., Dilcher, D.L., 1996. Oak leaves as biosensors of late Neogene and early Pleistocene paleoatmospheric CO_2 concentrations. Mar. Micropaleontol. 27, 299–312.

Lancucka-Środoniova, M., 1966. Tortonian flora from the "Gdów Bay" in the south of Poland. Acta Palaeobot. 7, 1–135.

Lunt, D.J., Jones, T.D., Heinemann, M., Huber, M., LeGrande, A., Winguth, A., Loptson, C., Marotzke, J., Roberts, C.D., Tindall, J., Valdes, P., Winguth, C., 2012. A model–data comparison for a multi-model ensemble of early Eocene atmosphere–ocean simulations: EoMIP. Clim. Past 8, 1717–1736.

Manum, S., 1966. *Ginkgo spitsbergensis* n.sp. from the Paleocene of Spitsbergen and a discussion of certain Tertiary species of *Ginkgo* from Europe and North America. Norsk Polarinstitut Årbok, 1955, pp. 49–58.

Mays, C., Steinthorsdottir, M., Stilwell, J.D., 2015. Climatic implications of *Ginkgoites waarrensis* Douglas emend. from the south polar Tupuangi flora, Late Cretaceous (Cenomanian), Chatham Islands. Palaeogeogr. Palaeoclimatol. Palaeoecol. 438, 308–326.

McElwain, J.C., Mayle, F.E., Beerling, D.J., 2002. Stomatal evidence for a decline in atmospheric CO_2 concentration during the Younger Dryas stadial: a comparison with Antarctic ice core records. J. Quat. Sci. 17, 21–29.

Mösle, B., Collinson, M.E., Finch, P., Stankiewicz, B.A., Scott, A.C., Wilson, R., 1998. Factors influencing the preservation of plant cuticles: a comparison of morphology and chemical composition of modern and fossil examples. In: Harsfield, B., Rohde, M., Schaefer, R.G., Wilkes, H. (Eds.), Advances in Organic Geochemistry. Eighteenth International Meeting of Organic Geochemistry. Proceedings. Part II: Biogeochemistry. Organic Geochemistry, pp. 1369–1380.

Neftel, A., Moor, E., Oeschger, H., Stauffer, B., 1985. Evidence from polar ice cores for the increase in atmospheric CO_2 in the past two centuries. Nature 315, 45–47.

Overdieck, D., Strassemeyer, J., 2005. Gas exchange of *Ginkgo biloba* leaves at different CO_2 concentration levels. Flora 200, 159–167.

Poole, I., Kürschner, W., 1999. Stomatal density and index: the practice. In: Jones, T.P., Rowe, N.P. (Eds.), Fossil Plants and Spores, Modern Techniques. Geological Society of London, London, pp. 257–260.

Quan, C., Sun, C., Sun, Y., Sun, G., 2009. High resolution estimates of paleo-CO_2 levels through the Campanian (Late Cretaceous) based on Ginkgo cuticles. Cretac. Res. 30, 424–428.

Retallack, G.J., 2001. A 300-million year record of atmospheric carbon dioxide from fossil plant cuticles. Nature 411, 287–290.

Retallack, G.J., 2002. Carbon dioxide and climate over the past 300 Myr. Philos. Trans. R. Soc. Lond. Ser. A, Math. Phys. Eng. Sci. 360, 659–673.

Roth-Nebelsick, A., Oehm, C., Grein, M., Utescher, T., Kunzmann, L., Friedrich, J.P., Konrad, W., 2014. Stomatal density and index data of *Platanus neptuni* leaf fossils and their evaluation as a CO_2 proxy for the Oligocene. Rev. Palaeobot. Palynol. 206, 1–9.

Royer, D.L., 2003. Estimating latest Cretaceous and Tertiary atmospheric CO_2 from stomatal indices. In: Wing, S.L., Gingerich, P.D., Schmitz, B., Thomas, E. (Eds.), Causes and Consequences of Globally Warm Climates in the Early Paleogene. Geological Society of America, Boulder, Colorado, pp. 79–93.

Royer, D.L., 2014. Personal communication. Department of Earth and Environmental Sciences, Wesleyan University. USA.

Royer, D.L., Hickey, L.J., Wing, S.L., 2003. Ecological conservatism in the "living fossil" Ginkgo. Paleobiology 29, 84–104.

Royer, D.L., Wing, S.L., Beerling, D.J., Jolley, D.W., Koch, P.L., Hickey, L.J., Berner, R.A., 2001. Paleobotanical evidence for near present-day levels of atmospheric CO_2 during part of the Tertiary. Science 292, 2310–2313.

Rundgren, M., Bennike, O., 2002. Century-scale changes of atmospheric CO_2 during the last interglacial. Geology 30, 187–189.

Sagoo, N., Valdes, P., Flecker, R., Gregoire, L.J., 2013. The Early Eocene equable climate problem: can perturbations of climate model parameters identify possible solutions? Philos. Trans. R. Soc. A 371, 20130123.

Siegenthaler, U., Stocker, T.F., Monnin, E., Luthi, D., Schwander, J., Stauffer, B., Raynaud, D., Barnola, J.-M., Fischer, H., Masson-Delmotte, V., Jouzel, J., 2005. Stable carbon cycle – climate relations during the late Pleistocene. Science 310, 1313–1317.

Smith, R.Y., Greenwood, D.R., Basinger, J.F., 2010. Estimating paleoatmospheric pCO_2 during the Early Eocene Climatic Optimum from stomatal frequency of *Ginkgo*, Okanagan Highlands, British Columbia, Canada. Palaeogeogr. Palaeoclimatol. Palaeoecol. 293, 120–131.

Steinthorsdottir, M., Jeram, A.J., McElwain, J.C., 2011. Extremely elevated CO_2 concentrations at the Triassic/Jurassic boundary. Palaeogeogr. Palaeoclimatol. Palaeoecol. 308, 418–432.

Steinthorsdottir, M., Wohlfarth, B., Kylander, M.E., Blaauw, M., Reimer, P.J., 2013. Stomatal proxy record of CO_2 concentrations from the last termination suggests an important role for CO_2 at climate change transitions. Quat. Sci. Rev. 68, 43–58.

Szafer, W., 1961. Miocénska flora ze Starych Gliwic na lásku (Miocene flora from Stare Gliwice in upper Silesia). Institut Geologiczny Prace 33, 1–205.

Tralau, H., 1968. Evolutionary trends in the genus *Ginkgo*. Lethaia 1, 63–101.

Upchurch, G.R., Kiehl, J., Shields, C., Scherer, J., Scotese, C.R., 2015. Latitudinal temperature gradients and high-latitude temperatures during the latest Cretaceous: congruence of geologic data and climate models. Geology 43, 683–686.

van de Water, P.K., Leavitt, S.W., Betancourt, J.L., 1994. Trends in stomatal density and $^{13}C/^{12}C$ ratios of *Pinus flexilis* during the last glacial–interglacial cycle. Science 264, 239–242.

Van der Burgh, J., Visscher, H., Dilcher, D.L., Kürschner, W.M., 1993. Paleoatmospheric signatures in Neogene fossil leaves. Science 260, 1788–1790.

van Hoof, T.B., Kaspers, K.A., Wagner, F., van de Wal, R.S.W., Kurschner, W.M., Visscher, H., 2005. Atmospheric CO_2 during the 13th century AD: reconciliation of data from ice core measurements and stomatal frequency analysis. Tellus, Ser. B Chem. Phys. Meteorol. 57, 351–355.

Wagner, F., Below, R., de Klerk, P., Dilcher, D.L., Joosten, H., Kurschner, W.M., Visscher, H., 1996. h CO_2 increase. Proc. Natl. Acad. Sci. USA 93, 11705–11708.

Wagner, F., Bohncke, S.J.P., Dilcher, D.L., Kurschner, W.M., van Geel, B., Visscher, H., 1999. Century-scale shifts in early Holocene atmospheric CO_2 concentration. Science 284, 1971–1973.

Wagner, F., Dilcher, D.L., Visscher, H., 2005. Stomatal frequency responses in hardwood-swamp vegetation from Florida during a 60-year continuous CO_2 increase. Am. J. Bot. 92, 690–695.

Woodward, F.I., 1987. Stomatal numbers are sensitive to increases in CO_2 from preindustrial levels. Nature 327, 617–618.

Wynn, J.G., 2003. Towards a physically based model of CO_2-induced stomatal frequency response. New Phytol. 157, 394–398.